Genetic removal of p70 S6K1 corrects coding sequence length-dependent alterations in mRNA translation in fragile X syndrome mice

Sameer Aryal[a,b], Francesco Longo[b], and Eric Klann[b,c,1]

[a]Sackler Institute of Graduate Biomedical Sciences, New York University School of Medicine, New York, NY 10016; [b]Center for Neural Science, New York University, New York, NY 10003; and [c]New York University Langone Health's Neuroscience Institute, New York University School of Medicine, New York, NY 10016

Edited by Nahum Sonenberg, McGill University, Montreal, QC, Canada, and approved March 17, 2021 (received for review February 5, 2020)

Loss of the fragile X mental retardation protein (FMRP) causes fragile X syndrome (FXS). FMRP is widely thought to repress protein synthesis, but its translational targets and modes of control remain in dispute. We previously showed that genetic removal of p70 S6 kinase 1 (S6K1) corrects altered protein synthesis as well as synaptic and behavioral phenotypes in FXS mice. In this study, we examined the gene specificity of altered messenger RNA (mRNA) translation in FXS and the mechanism of rescue with genetic reduction of S6K1 by carrying out ribosome profiling and RNA sequencing on cortical lysates from wild-type, FXS, S6K1 knockout, and double knockout mice. We observed reduced ribosome footprint (RF) abundance in the majority of differentially translated genes in the cortices of FXS mice. We used molecular assays to discover evidence that the reduction in RF abundance reflects an increased rate of ribosome translocation, which is captured as a decrease in the number of translating ribosomes at steady state and is normalized by inhibition of S6K1. We also found that genetic removal of S6K1 prevented a positive-to-negative gradation of alterations in translation efficiencies (RF/mRNA) with coding sequence length across mRNAs in FXS mouse cortices. Our findings reveal the identities of dysregulated mRNAs and a molecular mechanism by which reduction of S6K1 prevents altered translation in FXS.

fragile X syndrome | mRNA translation | translation elongation | protein synthesis | autism

Loss of expression or function of the fragile X mental retardation protein (FMRP) causes fragile X syndrome (FXS), the most prevalent inherited form of intellectual disability and the leading monogenic cause of autism. FMRP is an RNA-binding protein whose primary function is widely believed to be to repress messenger RNA (mRNA) translation in neurons. Accordingly, elevated net de novo protein synthesis is observed in the brains of FXS model mice (1). Precise control of translation is especially critical in the brain because rapid protein synthesis underlies long-lasting synaptic plasticity, multiple forms of which are impaired in FXS mice (2). There is consensus that dysregulated translation underlies a majority of phenotypes exhibited by FXS mice, including autism-like behaviors (3). Restoring translational homeostasis in the brain therefore presents an attractive therapeutic concept in FXS. Accordingly, genetic deletion of the translation stimulator p70 S6 kinase 1 (S6K1) in FXS mice rescues multiple phenotypes, including exaggerated translation, aberrant synaptic plasticity and dendritic morphology, and autism-like behaviors (4). Given that aberrant mRNA translation is a core pathophysiology of FXS, and that restoring translational homeostasis corrects pathological phenotypes, it is evident that one way to understand the molecular basis of FXS is to 1) identify mistranslated mRNAs, 2) ascertain the mechanism(s) by which the translation of these mRNAs is altered in FXS, and 3) establish how these translation mechanisms are corrected in models of FXS rescue.

Several studies have attempted to identify aberrantly translated mRNAs in FXS mice (5–7). Intriguingly, all three analyses noted that a large fraction of differentially translated genes showed reduced ribosome association in FXS. Although several explanations have been offered for this puzzling finding, a recent study observing similar reductions in ribosome association with depletion of FMRP in *Drosophila* oocytes led its authors to challenge the dogma that FMRP loss causes increased de novo protein synthesis (8). There is also limited overlap among the genes identified as aberrantly translated in the studies, necessitating further investigations to clarify the translational targets of FMRP. Moreover, very little is known about the molecular mechanisms by which translational homeostasis is restored through genetic reduction of S6K1 in FXS mice.

In this study, we sought to identify the mRNAs that are mistranslated in FXS mouse brains, ascertain the molecular basis of the alteration in translation, and investigate the mechanism by which genetic deletion of S6K1 normalizes the aberrant translation to levels observed in wild-type (WT) littermates. We carried out ribosome profiling and RNA sequencing (RNA-Seq) on cortical lysates from ∼P30 WT, FXS, S6K1 knockout, and double knockout (DKO) mice. Consistent with previous studies, we observed that the majority of genes with differential ribosome association in FXS displayed reduced ribosome footprint (RF) abundance. Using molecular assays, we discovered evidence that this reduction reflects a global increase in the rate of ribosome translocation in FXS neurons, is captured by a decreased number of translating ribosomes at steady state, and is normalized by

Significance

Fragile X syndrome (FXS) is the most prevalent inherited form of intellectual disability. FXS is caused by loss of fragile X mental retardation protein (FMRP), an RNA-binding protein that represses translation. Correspondingly, genetic removal of the translation-stimulating p70 S6 kinase 1 (S6K1) in FXS mice restores translational homeostasis and rescues synaptic and behavioral phenotypes. However, the mechanisms of FMRP function are in dispute, and the molecular basis of the rescue in protein synthesis with reduction of S6K1 is unknown. Here, by carrying out ribosome profiling and molecular assays, we reveal the molecular mechanisms by which reduction of S6K1 corrects altered protein synthesis in FXS. Our study elucidates the molecular foundations of a model for correction of pathophysiological features of FXS.

Author contributions: S.A., F.L., and E.K. designed research; S.A. and F.L. performed research; S.A. analyzed data; and S.A. and E.K. wrote the paper.

The authors declare no competing interest.

This article is a PNAS Direct Submission.

[1]To whom correspondence may be addressed. Email: eklann@cns.nyu.edu.

This article contains supporting information online at https://www.pnas.org/lookup/suppl/doi:10.1073/pnas.2001681118/-/DCSupplemental.

Published April 27, 2021.

pharmacological inhibition of S6K1. We also observed that alterations in RF abundance and mRNA expression show opposing associations with coding sequence (CDS) length in FXS mice and summate as a positive-to-negative linear gradation in log-fold changes (LFCs) in translation efficiency (TE, RF/mRNA) with CDS length. Remarkably, this gradation is prevented by the genetic removal of S6K1 in FXS mice. Therefore, we have uncovered the identities of mistranslated mRNAs in FXS, the mechanistic basis of aberrant translation and a molecular mechanism for correction of de novo protein synthesis with genetic reduction of S6K1 in FXS mice.

Results

To investigate the impact of FMRP loss on the translation of specific mRNAs, we first examined polysome profiles prepared from cortical lysates from P30 FXS mice. We observed little difference in the polysome profiles of FXS mice compared to WT littermates (*SI Appendix*, Fig. S1*A*). We proceeded to perform ribosome profiling to infer mRNA translation profiles at a genome-wide level (*SI Appendix*, Fig. S1*B*) (9). The majority (n = 153) of the 204 genes with significantly altered RF abundance in FXS cortices showed reduced footprint counts (Fig. 1*A*) and were enriched for genes linked to glial cell development (Fig. 1*F*). In stark contrast, of the 351 genes with significantly changed mRNA expression, the majority (n = 265) showed elevated expression in FXS brains (Fig. 1*A*, n = 4 FXS, 4 WT) and were enriched for genes implicated in synaptic transmission and development of the nervous system (Fig. 1*F*).

The genes with aberrant RF abundance in FXS brains overlapped significantly ($P = 2.0 \times 10^{-3}$), albeit weakly (n = 26), with previously identified binding targets of FMRP (10). In addition, all overlapping genes exhibited reductions in RF abundance in FXS. In contrast, the genes with altered mRNA expression showed a robust overlap with FMRP targets (n = 131, $P = 4.5 \times 10^{-66}$), with almost all (n = 129) exhibiting increased mRNA expression in FXS brains.

Previous work has suggested that the translation of mRNAs with long CDSs is particularly vulnerable to FMRP loss (7, 8). To evaluate this phenomenon, we ordered mRNAs ascendingly by their CDS lengths, divided them into six color-coded bins, and evaluated their (LFCs) against their false discovery rate (FDR)-adjusted P values (Fig. 1*B*). Among mRNAs with significantly decreased RF abundance in FXS cortices, we observed enrichment for those with long CDSs. Conversely, mRNAs with short CDSs exhibited a significant up-regulation of RFs. Analyzing the fold changes of all mRNAs revealed that as the CDS length of an mRNA increases, it is more likely to exhibit reduced RF abundance in FXS brains, with the mRNAs harboring the shortest CDSs showing up-regulation of footprints (Fig. 1*D*). Meanwhile, identical analysis of mRNA expression showed opposite associations. mRNAs with long CDSs were up-regulated in FXS brains, whereas mRNAs with short CDSs were down-regulated (Fig. 1*C*). Analyzing transcriptome-wide fold changes revealed that the probability of elevation in mRNA expression was a positive function of CDS length: As the CDS length of mRNA is extended, it is more likely to increase in expression in FXS brains (Fig. 1*E*). Furthermore, the opposing effects in RF abundance and mRNA expression summate additively to elevate the LFCs in TE in FXS brains (Fig. 1*G* and *SI Appendix*, Fig. S1*C*). As expected, evaluating the cumulative probabilities of LFCs in TE against CDS lengths transcriptome-wide revealed a profile reminiscent to that of RF abundances but with elevated changes in each CDS length bin (Fig. 1*H*).

To confirm that our results were not artifacts of prespecified binning thresholds, and to directly compare the CDS length-dependent alterations in RF abundance and mRNA expression in FXS, we ordered mRNAs into 50 bins by their CDS length, with each bin harboring the same number of mRNAs. Evaluating the average LFC in each bin confirmed that mRNAs with shorter CDSs exhibit elevated RF abundance in FXS, and those with longer CDSs exhibit reduced RF abundance (Fig. 1*I*). It also validated the exact opposite trend for mRNA expression: mRNAs with shorter CDSs are reduced in FXS brains, while mRNAs with longer CDSs are elevated (Fig. 1*I*). Remarkably, both of these effects are linear: As CDS length increases, the magnitude of the alterations in RF abundance and mRNA expression in FXS brains exhibit negative and positive proportional changes, respectively. The combination of the positive-to-negative gradation in LFCs in RF abundance and the negative-to-positive variation in fold changes in mRNA expression with CDS length results in an even stronger positive-to-negative relationship between TE and CDS length in FXS brains (Fig. 1*J*). Importantly, we also observed strikingly similar results when we implemented our analysis on a previously published ribosome profiling and RNA-Seq dataset from P24 FXS model mouse brains (*SI Appendix*, Fig. S2) (7).

A straightforward interpretation of the reduction in RF counts in the majority of altered mRNAs would be that FMRP loss reduces mRNA translation (8). However, examination of cortical protein levels of several altered mRNAs with particularly long or short CDSs revealed either significant up-regulation or a trend toward up-regulation in FXS mice (Fig. 2*A*). Given evidence suggesting that FMRP directly binds to the ribosome (11) and stalls its translocation on specific mRNAs (10), we decided to further investigate the molecular basis of these observations. First, we examined de novo protein synthesis in embryonic cortical neurons from FXS mice. To label newly synthesized proteins, we used puromycin, an aminoacyl-transfer RNA (tRNA) analog that covalently binds nascent peptide chains and causes their premature release. Quantifying these truncated peptides measures de novo protein synthesis (12), which we observed to be elevated in FXS primary neurons (Fig. 2 *B* and *C*).

To examine protein synthesis specifically during the elongation phase of translation, we pulsed FXS neurons with Harringtonine (HHT) for 0, 8, or 16 min, then chased them with puromycin (Fig. 2*F*). HHT inhibits translation initiation rapidly (13). Therefore, after its addition, puromycin labeling specifically measures the elongation phase of protein synthesis. Using this approach, hereafter called "elongation SUnSET" (ES), we observed elevated elongation-specific protein synthesis at baseline (where HHT and puromycin are added simultaneously) in FXS neurons (Fig. 2 *D* and *E*). Conversely, we observed a mild reduction in elongation-specific protein synthesis at baseline in FXS mouse embryonic cortical neurons transduced with human homolog of full-length FMRP (*SI Appendix*, Fig. S3 *A* and *B*). These results establish that de novo protein synthesis is elevated in FXS neurons even after inhibition of translation initiation, consistent with previous work showing that FMRP loss leads to a global elevation in elongation-specific protein synthesis in cortical lysates (14). However, one might also expect a similar outcome if FMRP loss led to increased initiation, in which mRNAs are already engaged with an increased number of ribosomes before HHT addition (*SI Appendix*, Fig. S4*B*). Intriguingly, comparing the elongation-specific protein synthesis in each condition against its own baseline (to examine the rate of decrease) revealed a significant reduction in puromycin signal in FXS neurons after 16 min of runoff elongation (*SI Appendix*, Fig. S4*A*). Conversely, we observed a mild increase in elongation-specific protein synthesis after 16 min of runoff elongation in FXS neurons transduced with human FMRP (*SI Appendix*, Fig. S3*C*). These results raised the possibility that there are far fewer ribosomes remaining to carry out protein synthesis after 16 min of runoff elongation in FXS neurons, which may explain why,

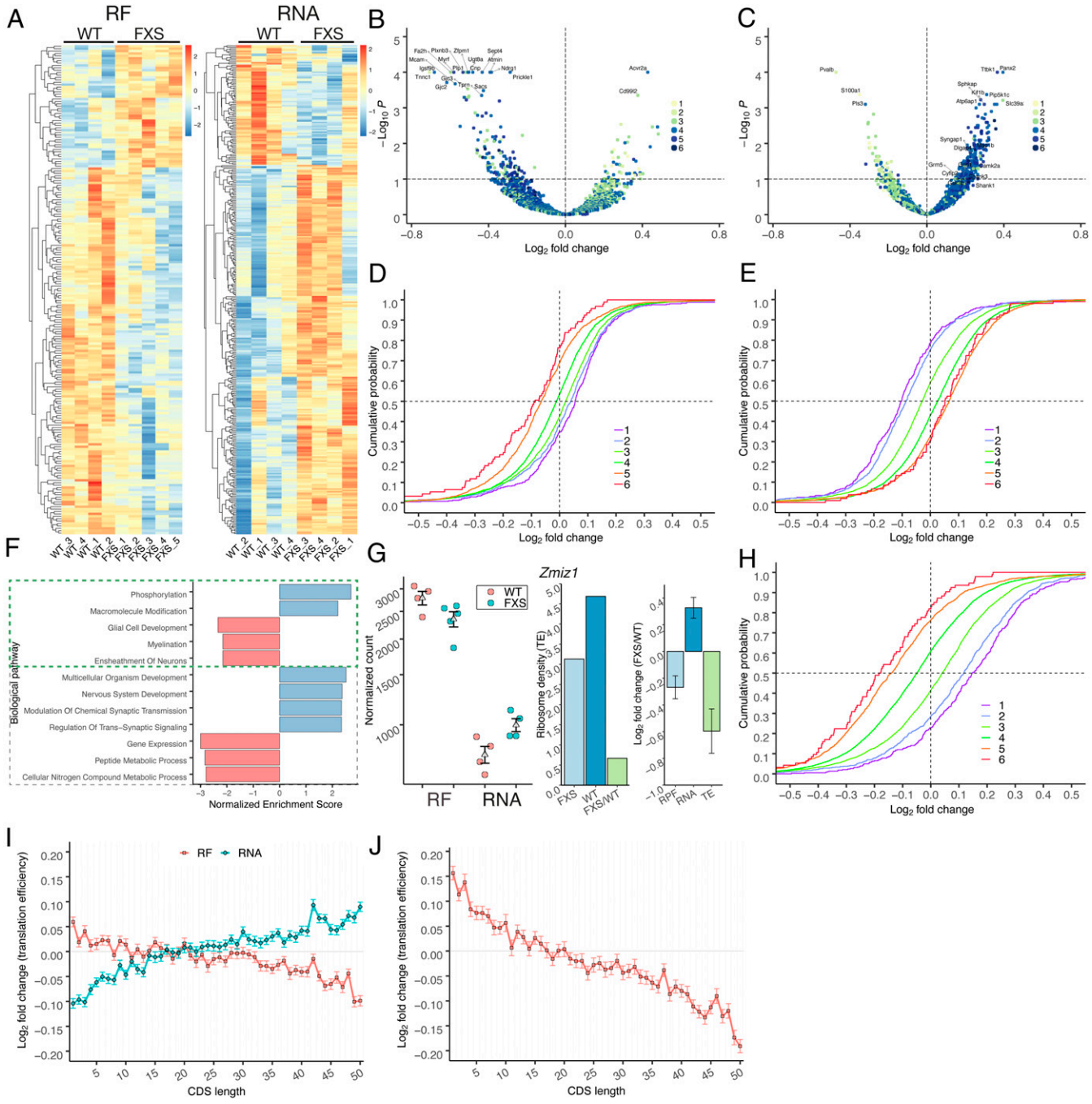

Fig. 1. Increased CDS length is associated with decreased RF abundance and increased mRNA expression in FXS mouse cortices. (*A*) Heat maps depicting RF abundance (n = 204) and mRNA expression (n = 351) of significantly different genes (FDR-adjusted P value< 0.1) between WT and FXS mouse cortices in ribosome profiling (*Left*) and RNA-Seq analyses (*Right*). Each row displays centered and scaled ("row-normalized") transcripts per million values for significantly different genes. (*B*) Significance (FDR-adjusted P value) versus LFC in RF abundance between FXS and WT mice. The 20 most significant genes are labeled. (*C*) Volcano plot of mRNA expression changes in FXS and WT mice. The top 10 significantly different genes and several genes previously shown to be implicated in FXS are labeled. (*D*) Cumulative distribution of LFCs in RF abundance (FXS/WT) as a function of CDS length (n = 415, 764, 3,494, 5,866, 1,451, and 93 mRNAs in bins 1 through 6). (*E*) Cumulative distribution of LFCs in mRNA expression (FXS/WT) as a function of CDS length (n = 434, 816, 3,713, 6,252, 1,556, and 105 mRNAs in bins 1 through 6). (*F*) Top biological processes enriched in FXS and WT mouse cortical tissue in ribosome profiling (upper green-dashed box) or RNA-Seq assays. (*G*) The translation profile of the *Zmiz1* gene. The RF abundance LFC (FXS/WT) and the negative of the mRNA expression LFC (FXS/WT) are added to calculate the LFC in TE. (*H*) Cumulative distribution of LFCs in translation efficiencies (FXS/WT) as a function of CDS length. Comparison of LFCs in RF abundance and mRNA expression (*I*) and TE (*J*) by CDS length in FXS. mRNAs are divided into 50 bins by their CDS lengths. Each bin contains ~250 mRNAs.

despite elevation at baseline, FXS neurons show reduction in elongation-specific protein synthesis after runoff.

To examine ribosome engagement specifically, we employed the ribopuromycylation method (RPM) (15). This assay uses puromycin to tag nascent proteins in the presence of emetine, a translation elongation inhibitor that freezes ribosomes in place on mRNAs without affecting its catalytic activity. Because emetine rescues the ribosome from puromycin-induced dissociation,

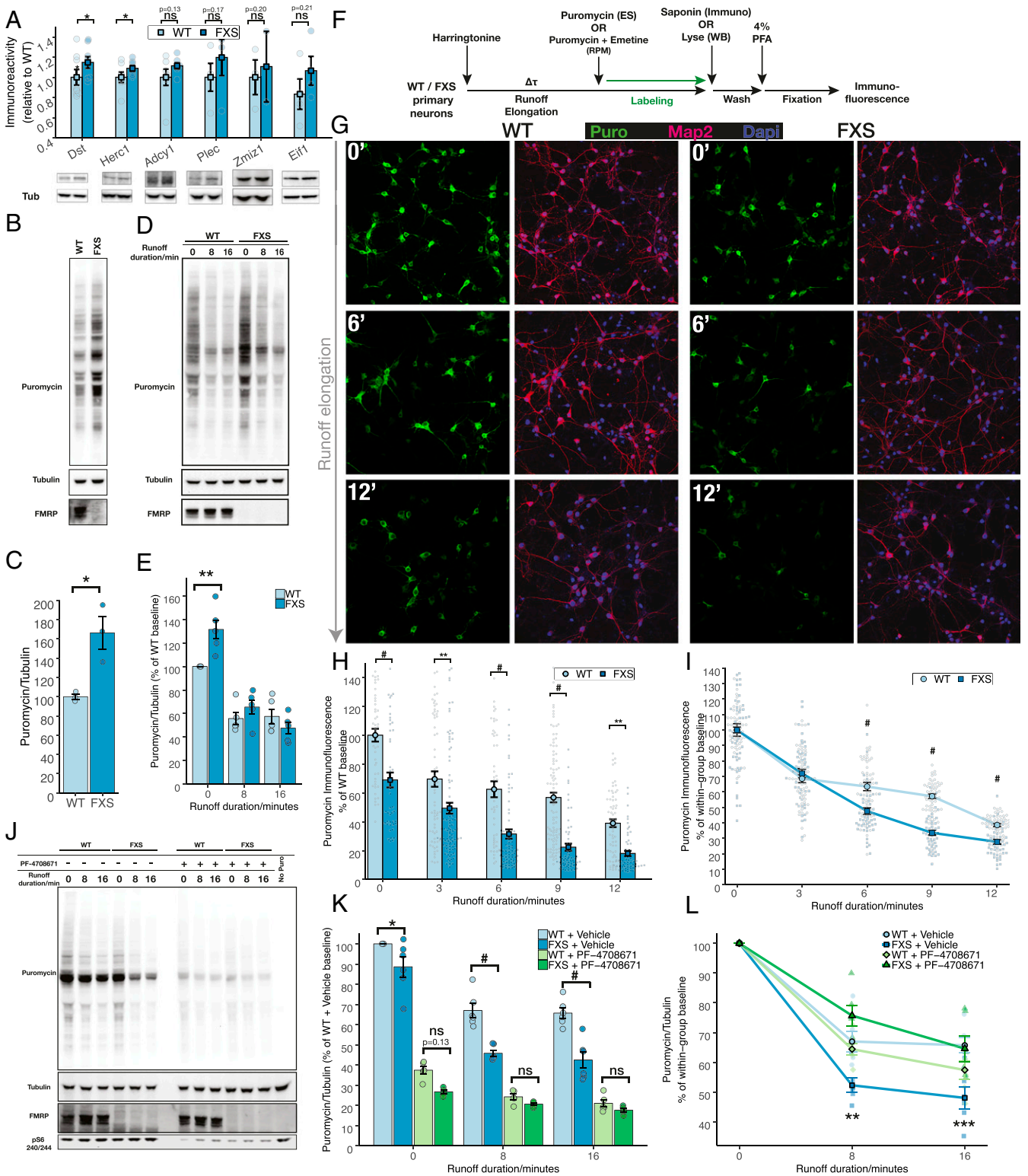

Fig. 2. The rate of translation elongation is increased in FXS primary neurons and is sensitive to the inhibition of S6K1. (*A*) Representative immunoblots and their quantifications examining the protein levels of mRNAs with particularly long (Dst, Herc1, Adcy1, Plec, and Zmiz1) or short (Eif1) CDSs in cortical lysates from WT and FXS mice. (*B*) Representative Western blot of WT and FXS cortical neurons incubated with puromycin. (*C*) Quantification of *A* (*t* test, $P = 0.05$). (*D*) Representative Western blot of the ES assay in WT and FXS neurons. (*E*) Quantification of *C* (pairwise *t* test, holm-adjusted $P = 0.007$ at baseline). (*F*) Protocol for ES and runoff-RPM assays. (*G*) Representative immunofluorescence images of runoff-RPM in WT and FXS mouse cortical cultures. (*H*) Quantification of *G* across two experiments. (*I*) Results from *H*, expressed as a percentage of its own baseline. (*J*) Representative Western blot of runoff-RPM assay in WT and FXS mouse neurons treated with the S6K1 inhibitor PF-4708671. (*K*) Quantification of *G*. Values are expressed as a percentage of WT + vehicle baseline. (*L*) The inverse of the rate of runoff elongation. Elongation rate is increased in FXS (t8, WT + vehicle versus FXS + vehicle, holm-adjusted $P = 0.005$) and is rescued by pharmacological inhibition of S6K1 (pairwise *t* test, t16 WT + vehicle versus t16 FXS + PF470861 holm-adjusted $P = 1$). #$P < 0.001$, **$P < 0.01$, *$P < 0.1$, ns: $P > 0.1$. Pairwise *t* test used for post hoc comparisons with holm adjustment.

each translating ribosome is tagged with a single molecule of puromycin. We reasoned that pulsing cultured neurons with HHT and chasing with RPM would permit measurement of the number of translating ribosomes remaining after defined periods of runoff elongation (Fig. 2*F*). To examine whether this approach was feasible, we first carried out RPM on human embryonic kidney (HEK) 293 cells. Probing for puromycin revealed a clear cytoplasmic signal that was dramatically reduced by a 15 min preincubation with anisomycin or HHT (*SI Appendix*, Fig. S4*C*). Pulsing HEK293 cells with HHT for 0, 5, 10, or 15 min, chasing with RPM, and probing for puromycin on immunoblots revealed an anisomycin and runoff elongation-dependent decrease in puromycin signal (*SI Appendix*, Fig. S4*D*). These results suggested that the combination of HHT and RPM could be used to probe actively translating ribosomes during runoff elongation in cultured neurons, which also showed an anisomycin and runoff elongation-dependent reduction in RPM signal (*SI Appendix*, Fig. S4*E*). Using this approach, hereafter termed "runoff-RPM," we observed reduced levels of translating ribosomes in FXS neurons at baseline (Fig. 2 *G* and *H* and *SI Appendix*, Fig. S4*F*). With increasing runoff durations of 3, 6, 9 and 12 min, we observed further reductions in the number of translating ribosomes in FXS neurons (Fig. 2 *G* and *H* and *SI Appendix*, Fig. S4*F*). Determining the rate of loss in the number of translating ribosomes, which we computed by comparing the number of translating ribosomes remaining after runoff elongation in each condition against its own baseline, revealed a faster rate of decrease in the RPM signal with runoff elongation in FXS neurons (Fig. 2*I*). Conversely, with increased runoff elongation, we observed a slower rate of decrease in the number of translating ribosomes in FXS neurons transduced with human FMRP (*SI Appendix*, Fig. S5 *A–C*). These results strongly suggest that FMRP impedes ribosome translocation and that its loss causes a global increase in the rate of translation elongation in neurons.

To better understand how S6K1 regulates translation in FXS, we carried out runoff-RPM followed by Western blotting in WT and FXS cortical neurons treated with the S6K1 inhibitor PF-4708671. Consistent with the results from immunofluorescence studies, we observed a significant reduction in the number of ribosomes in FXS neurons treated with vehicle at baseline compared to WT neurons (Fig. 2 *J* and *K*). This effect was amplified with runoff elongation: Fewer translating ribosomes remained after 8 and 16 min of runoff elongation in FXS neurons. In contrast, the expression of human FMRP in FXS neurons elevated the number of ribosomes remaining after runoff elongation (*SI Appendix*, Fig. S5 *D–F*). Inhibition of S6K1 with PF-4708671 dramatically reduced the number of translating ribosomes at baseline in both WT and FXS neurons. However, with runoff elongation, the reductions observed in FXS neurons treated with PF-4708671 were not as substantial as those observed in vehicle-treated FXS neurons. Evaluating the rate of loss of the runoff-RPM signal, which quantifies the inverse of the rate of translation elongation, revealed that pharmacological inhibition of S6K1 rescues the excessive rate of translation elongation in FXS neurons (Fig. 2*L*). Combined, these results establish that an increase in the rate of ribosome translocation largely mediates elevated de novo protein synthesis in FXS neurons. This increase is captured by the reduced number of translating ribosomes with runoff elongation in FXS neurons, which in turn explains why the majority of altered genes in FXS brains have decreased RF counts.

Given our observation that inhibition of S6K1 rescues the rate of translation elongation in FXS neurons, we asked whether the previously observed genetic rescue with S6K1 deletion also was mediated by reducing the rate of elongation on specific mRNAs in vivo. We examined the RF abundance ($n = 3$) and mRNA expression ($n = 4$) of DKO mice that harbor genetic deletions of both *Fmr1* (FMRP) and *Rps6kb1* (S6K1, Fig. 3*A* and *SI Appendix*, Fig. S6*E*). To our surprise, the DKO mice exhibited significant departures from WT mice in both RF abundance (236↑ and 355↓, Fig. 3*B* and *SI Appendix*, Fig. S6*A*) and mRNA expression (945↑ and 666↓, Fig. 3*C* and *SI Appendix*, Fig. S6*A*) for a large number of genes. However, we did not observe any clear CDS length dependency among mRNAs with significantly altered RF abundance or mRNA expression in DKO brains. We confirmed this transcriptome-wide by analyzing cumulative probabilities against LFCs of RF abundance (Fig. 3*D*) and mRNA expression (Fig. 3*E*) in DKO cortices. To compare DKO mice directly to their FXS littermates, we ordered mRNAs into 50 bins by their CDS lengths and examined their fold changes compared to WT mice. We observed that genetic reduction of S6K1 in FXS mice specifically normalized the aberrant bin-wise deviations in mRNA expression (Fig. 3*F*) and TE (Fig. 3*G* and *SI Appendix*, Fig. S6*B*), particularly for genes with especially long or short CDSs. Furthermore, examining the RF abundance and mRNA expression in FXS and DKO brains of the genes in the final four bins revealed that genetic reduction of S6K1 corrects overall alterations in gene expression by moving the RF abundance (Fig. 3*H*), and especially mRNA expression (Fig. 3*I*), of the entire bulk of genes toward the WT, rather than by rescuing specific genes. Identical evaluation of genes in the first four bins also showed a strikingly concordant effect (*SI Appendix*, Fig. S6 *C* and *D*).

Discussion

The TE of an mRNA historically has been deduced by the number of polysomes bound to it (16). Remarkably, an inverse correlation between CDS length and TE—the longer the CDS length of a transcript, the lower its ribosome density—has been observed in multiple model systems ranging from the protozoan *Plasmodium falciparum* to human cells (17). This relationship therefore suggests a CDS length-dependent effect on translational control that might be shared across phyla.

Because each RF reports on a single ribosome bound to an mRNA, the total number of RF reads aligning to a transcript directly reflects the overall number of polysomes bound to that mRNA species. Using ribosome profiling and RNA-Seq, we uncovered a positive-to-negative gradation of alterations in TE in the cortices of FXS model mice. This gradation suggests that the mechanisms regulating CDS length-dependent control of translation go awry with the loss of FMRP.

How does CDS length control translation? Using an elegant mathematical model, Fernandes et al. (17) proposed that mRNAs with short CDSs exhibit an increased rate of translation initiation. They assumed that the local concentration of ribosomal subunits around the 5′ untranslated region (UTR) of an mRNA determines its initiation rate. The shorter the CDS, the closer the 5′ end of an mRNA is to its 3′ end. After translation terminates, the concentration of ribosomal subunits at the 5′ UTR is therefore higher for short CDS mRNAs, which increases the initiation rate on those mRNAs. Ingolia et al. (9), meanwhile, proposed that mRNAs with long CDSs exhibit an increase in the rate of translation elongation. Consistent with previous polysome profiling studies, these researchers observed that shorter genes tended to have higher ribosome densities. Examination of the average ribosome densities of thousands of mRNAs revealed a high ribosome density toward the 5′ end of their CDSs, which tapered off and persisted at a uniform level toward the 3′ end. This trend suggested that the reduction in ribosome density with CDS length may be mediated by a relative increase in the rate of elongation on distal parts of the transcript on long CDS mRNAs (9). Therefore, in the absence of any

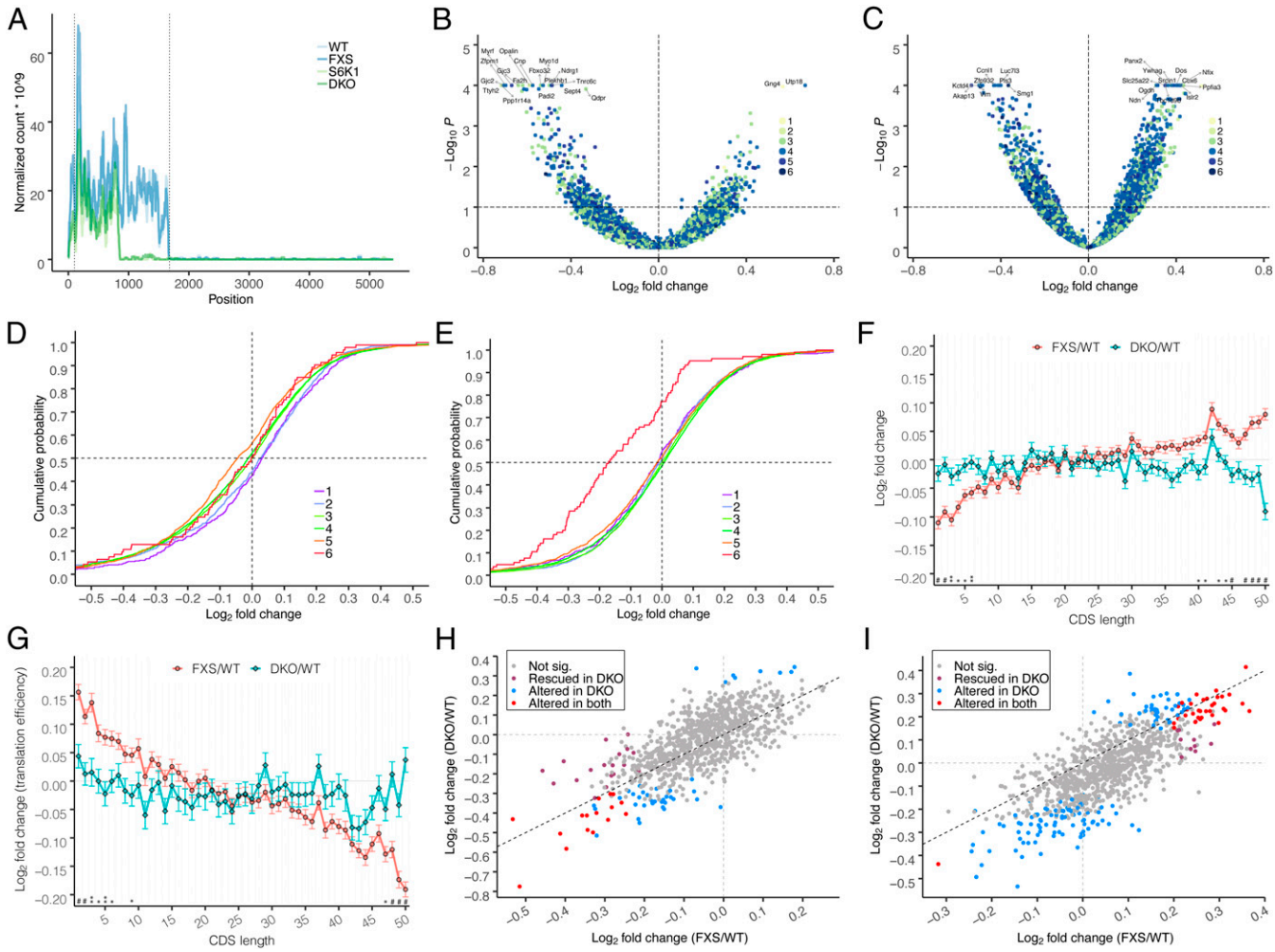

Fig. 3. CDS length dependency of TE and mRNA expression in FXS mouse cortices is corrected by genetic reduction of S6K1. (*A*) RF profile of *Rps6kb1* mRNA. Profile accurately captures the stop codon introduced to make the S6K1 deletion. Dotted lines indicate UTR boundaries. Volcano plot of RF abundance (*B*) ($n = 3$) and mRNA expression (*C*) ($n = 4$) (DKO/WT). The top 20 genes are labeled. Cumulative distribution of LFCs in RF abundance (*D*) and mRNA expression (*E*) in DKO brains, as a function of CDS length. Bin sizes are the same as those used in Fig. 1 *D* and *E*, respectively. Comparison of LFCs by CDS length in FXS and DKO brains in mRNA expression (*F*) and TE (*G*) datasets. Comparison of RF abundance (*H*) and mRNA expression (*I*) in FXS and DKO brains of genes in the longest four bins, compared to the WT. The majority of points are above the x = y line in RF abundance and below the line in RNA expression, suggesting a generalized reduction in RF abundance and mRNA expression toward WT levels. #$P < 0.001$, **$P < 0.01$, *$P < 0.1$. Kruskal–Wallis test used for comparison of LFCs within each bin; *P* values are holm-adjusted.

exogenous changes, mRNAs with short CDSs are likely to exhibit increased rates of initiation, while those with long CDSs are likely to exhibit increased rates of elongation.

If these two proposals were to be true, what would be the consequences if FMRP were genetically removed from this system? Using molecular assays, we have provided substantial confirmatory evidence that the rate of translation elongation is globally elevated in FXS. FMRP loss therefore likely causes elevated rates of elongation on mRNAs with short or long CDSs. On mRNAs with especially short CDSs, the increase in the rate of elongation would in turn increase the rate of termination and subsequently elevate the local concentration of ribosome subunits around their 5′ UTRs. This increase would cause further enhancement in the rate of translation initiation on those mRNAs. On mRNAs with long CDSs, the elevated rate of elongation would cause additional reductions in ribosome density. Importantly, both of these effects would be determined directly by CDS length. This model would therefore predict that loss of FMRP causes an elevation in the TEs of mRNAs with short CDSs, a reduction in the TEs of mRNAs with long CDSs, and a CDS length-dependent gradation between the two extremes. Remarkably, the predictions of this model exactly match the alterations we observed in the cortices of FXS mice. The positive-to-negative linear gradation of alterations in RF abundance and TE with CDS length may, therefore, be an emergent property of an increased rate of ribosome translocation in FXS.

Given that CDS length-dependent control of translation may be a general feature across phyla, it is worthwhile to consider what evolutionary advantages it may serve. It has long been known that mRNAs of housekeeping genes have particularly short CDSs (18). Housekeeping genes, by definition, are constitutively, and often robustly, expressed in all human cells. Given the large energetic costs of transcription, translation, and protein folding (19–21), it is possible that natural selection has favored shorter CDSs for constitutively expressed genes. The short length of the mRNA also might allow cells to respond to stimuli by rapidly increasing the transcription and/or translation

of these genes, thereby providing a benefit to respond rapidly to the environment.

Interestingly, housekeeping genes are enriched in mRNAs coding for components of the ribosome (18). Consistent with the model that FMRP exerts CDS length-dependent translational control, the short CDS mRNAs coding for ribosomal proteins are elevated in RF abundance and TE in FXS cortices (*SI Appendix*, Fig. S7). Conversely, there is evidence that FMRP binding partners are enriched in long mRNAs, which tend to harbor proportionately long CDSs (22). Again, consistent with the proposed model, FMRP binding partners exhibit reductions in RF abundance and TE in the cortices of mice lacking FMRP (*SI Appendix*, Fig. S7).

One limitation of the model proposed above is that the individual fold changes in RF abundance and mRNA expression are often small and are largely between ±1.3-fold. It is notable that despite the small individual effect sizes, we observe a linear gradation of alterations in RF abundance and mRNA expression. Because this analysis was carried out by examining the LFCs in over 12,000 mRNAs, it is very unlikely that such a gradation of effects would occur if the translation of only a limited number of mRNAs were affected in FXS. Our model therefore predicts that the vast majority of mRNAs are excessively translated in FXS cortices. This idea is consistent with the failure to find a specific motif or secondary structure for FMRP binding. Although studies have suggested that the ACUK motif is overrepresented in FMRP binding partners, it is improbable that it confers specificity to FMRP binding because it is present in every mRNA (11). Similarly, although it has been shown that the RGG box of FMRP binds to G-quadruplexes in vitro, the in vivo binding partners of FMRP do not show any enrichment for these secondary structures (10). It is therefore likely either that FMRP binds to a far larger number of mRNAs than is currently accepted or that its loss causes an indiscriminate increase in the rate of ribosome translocation on all mRNAs. Our data shows that this elevation is captured by the increase in de novo protein synthesis and is mediated by an overall increase in the rate of translation elongation.

It should also be noted that although we observed trends toward elevated protein expression of mRNAs with particularly long or short CDSs, we observed statistically significant elevations in the protein levels of only a small subset of the mRNAs we examined. We speculate that because de novo translation is elevated as a whole across the translatome, the effects on individual proteins are likely to be small; only when summated across the entire translatome are the effects robust. This reduction in the magnitude of effect sizes of individual proteins is evident in the small fold changes in RF abundance and mRNA expression, which are largely between 1.3- and −1.3-fold. Furthermore, using ribosome profiling and RNA-Seq, we only measured alterations in de novo translation in FXS cortices. The steady-state levels of individual proteins are determined by other factors as well, including their degradation kinetics, which make it challenging to validate the alterations by examining total protein levels in tissue lysates.

Another limitation of our model is that the alterations observed in both runoff-RPM and elongation SUnSET are more muted in the data comparing FXS neurons transduced with FMRP and those with GFP, as opposed to data comparing WT and FXS neurons. For instance, we observe a significant reduction in runoff-RPM signal at baseline in FXS neurons compared to WT (*SI Appendix*, Fig. S5 *D* and *E*). However, in FXS neurons transduced with human FMRP, the runoff-RPM signal at baseline is elevated, albeit without reaching statistical significance, compared to murine FXS neurons transduced with GFP. There are three reasons why this may happen. First, it is possible that human FMRP does not fully recapitulate the functions of mouse FMRP. Second, the amount of FMRP expressed virally may not be sufficient to fully rescue the deficits in translation observed in FXS neurons. Although we used strong, ubiquitously expressed promoters and observed robust Fl-FMRP expression in both immunofluorescence images and Western blots, we can only comment on the relative amount of FMRP expression and not on absolute amounts. Third, it is possible that FMRP is not expressed for long enough to fully recapitulate the effects of endogenous FMRP expression. In the experiment comparing WT and FXS neurons, endogenous FMRP is present throughout the duration of culture in FXS neurons, whereas in the viral transduction experiment, FMRP is present only for approximately 4 d. If FMRP loss causes systemic secondary alterations, it is possible that this duration of FMRP expression is too short to fully correct those changes.

It is also important to acknowledge that the bulk of evidence demonstrating an elevated rate of ribosome translocation in FXS was acquired from experiments on primary neurons lacking FMRP, while that determining altered CDS length control was obtained from cortical lysates. We chose to carry out cell biological experiments on cultured primary neurons for two reasons. First, the magnitudes of the effects on individual mRNAs were quite small. In the cerebral cortices of mice, neurons strongly express FMRP at P30; glial cells do not (23). Because glia are thought to be at least as abundant as neurons in cortical tissue (24), we reasoned that our signals were being diluted by glial cells, which—given their comparative absence of FMRP—likely do not show alterations between genotypes. We therefore moved to an ex vivo cortical culture model system. We carried out our cultures at E16 and E17, where the proportion of glial cells is minuscule. As a result, our cultures are almost entirely neuronal (for instance, in Fig. 2*G*, almost every cell stained for puromycin is also positive for Map2, which is a marker for neurons). Second, puromycin does not cross the blood brain barrier, which makes in vivo experiments far more challenging. Given the number of drugs, sequential steps involved and the constraint that intracerebroventricular infusions must be carried out very slowly, we were not able to implement the runoff-RPM assay in vivo.

Given our proposition that the loss of CDS length control of translation is likely the emergent mechanism for altered protein synthesis in FXS brains, it is remarkable that the genetic removal of S6K1 in FXS brains corrects this aberration. A reduction in the rate of elongation in DKO cortices is a molecular mechanism that would predict the rescue of alterations in CDS length control of translation in FXS. Consistent with this model, pharmacological inhibition of S6K1 corrected the increase in the rate of elongation in FXS neurons. However, the excitement of this finding was tempered by the observation that the LFCs in RF abundance in DKO cortices closely tracked those observed in FXS cortices, especially for mRNAs with the longest CDSs. Because reduced RF abundance likely reflects an increase in the rate of elongation, this correspondence suggests that the rate of ribosome translocation is not dampened by genetic removal of S6K1 in FXS mice. Instead, the rescue in CDS length control of translation in DKO cortices is primarily driven by the correction of the alterations in CDS length dependency of mRNA expression in FXS. This normalization is especially evident in mRNAs with the longest CDSs, the majority of which exhibit increases in FXS cortices but reductions in DKO cortices. However, it remains unclear how the rescue of CDS length dependency in mRNA expression arises.

The reduction of CDS length dependency of alterations in mRNA expression in DKO cortices suggests that S6K1 signaling modulates mRNA expression in FXS model mice. Increased phosphorylation of S6K1 and its canonical target S6 have been

observed in the hippocampus of FXS brains, suggesting that S6K1 is hyperactivated (25). Previous studies suggest that S6K1 is required for ribosome biogenesis (26), and tissues that lack both S6K1 and S6K2 display widespread reductions in the mRNA expression of genes regulating ribosome biogenesis (27). Given the decrease in mRNA expression of genes encoding ribosomal proteins in FXS mice and its correction in DKO mice, it is possible that a rescue of this transcriptional program plays a role in correcting de novo protein synthesis in DKO mice. It should be noted that although this mechanism may account for the correction of LFCs in mRNA expression in genes with the shortest CDSs, it does not explain how the overall LFCs in the longest genes are also corrected in DKO mice.

There is also evidence that S6K1 controls transcription by phosphorylating the cAMP response element binding (CREB) protein isoform CREM (28). In addition, hyperactive S6K1 alters mRNA expression by modulating the activity of S6K1 Aly/REF-like target (SKAR), a nuclear protein that has been proposed to couple transcription with pre-mRNA splicing and mRNA export (29). Thus, a reduction in S6K1-SKAR signaling in the DKO mice also could participate in the rescue of altered mRNA expression in the FXS mice.

Because FMRP is thought to bind only to ∼1,000 mRNAs, it is also possible that the global increase in elongation rate is caused by a generalized increase in ribosome translocation due to hyperactivation of mammalian target of rapamycin complex 1 (mTORC1) to S6K1 signaling, which has been previously noted in FXS brains (25). This framework is consistent with the limited, albeit significant, overlap between genes with altered RF abundance and FMRP-binding targets and the reduction in the rate of translation elongation with inhibition of S6K1 in FXS neurons. Meanwhile, increased translation initiation due to elevated mTORC1 signaling to its other major downstream targets (4E-BP and/or CYFIP1) and resulting increases in eIF4F formation (30) explain the increase in footprint expression in the shortest genes. These genes are highly enriched in 5′ terminal oligopyrimidine mRNAs, which code for ribosomal proteins and are established translational targets of mTORC1 activation (*SI Appendix*, Fig. S7) (31). The positive-to-negative gradation in RF abundance and TE with CDS length argues for a model in which elevated rates of both initiation and elongation act in concert to elevate mRNA translation indiscriminately in FXS brains. It is possible that precisely because initiation is rate limiting, its increase is best captured in mRNAs with short CDSs. Meanwhile, the higher rate of elongation dominates in longer transcripts because ribosomes must translocate through a greater number of codons, with the net effect of each increased translocation event aggregating over the length of the CDS. Our proposed models are consistent with and provide mechanistic insights into previously proposed models of FMRP function (7, 11, 25, 30). Alternatively, it is possible that FMRP binding is more promiscuous than appreciated and biased toward longer mRNAs, which are enriched in neurons (32). Therefore, the increased rate of elongation is primarily observed in longer transcripts, and the secondary effect of increased rate of initiation is observed in shorter transcripts, which are translational targets of mTORC1 (*SI Appendix*, Fig. S7*B*).

Elevated rates of ribosome translocation also have been associated with increased mRNA stability (33). Specifically, an increase in the rate of decoding of cognate tRNAs at the ribosomal A site is thought to drive increases in mRNA stability. Because this process is likely elevated in every codon in FXS (7), the effect on mRNA stability is naturally summated over the length of a transcript. Notwithstanding the limitation that our experiments examining translation elongation were carried out in cultured neurons, this model accounts for the increased expression of mRNAs with long CDSs in FXS brains, as well as the negative-to-positive gradation in mRNA expression by CDS length.

Finally, based on our ex vivo findings with inhibition of S6K1, we speculate that genetic reduction of S6K1 causes destabilization of mRNAs in FXS mice. Recent work has demonstrated that reduction of cap-binding complex formation, which reduces translation initiation, causes a global reduction in mRNA stability (34). These findings are consistent with studies that showed a reduction in the stability and elevation of nonsense-mediated decay of specific transcripts upon inhibition of mTORC1 (35–38). Because it stimulates both initiation and elongation, it is possible that the genetic reduction of S6K1 causes a similar destabilization of mRNAs in DKO mice.

In addition to establishing bona fide targets for pharmacological interventions in FXS, our results ascertain the underlying biological principles of FMRP function in health and disease. Our work also suggests that drugs that reduce translation elongation on specific target mRNAs (39) may offer a therapeutic avenue in FXS.

Materials and Methods

Mouse Breeding. DKO mice were generated initially by crossing heterozygous female FXS mice carrying the *Fmr1* mutation with heterozygous male mice carrying the S6K1 mutation. Subsequently, all animals used for experimentation were derived from the crossing of female $X^{Fmr1}X^{+}$;S6K1/+ with either X^{+}Y;S6K1/+ or X^{Fmr1}Y;S6K1/+ males (4). All experimental animals were littermates. All procedures involving animals were performed in accordance with protocols approved by the New York University Animal Welfare Committee and followed the NIH *Guide for the Care and Use of Laboratory Animals* (40). All mice were housed in the New York University animal facility and were compliant with the NIH *Guide for the Care and Use of Laboratory Animals*. Mice were housed with their littermates in groups of two to three animals per cage and kept on a 12-h regular light/dark cycle, with food and water provided ad libitum.

Polysome Profiling. Cortices from P29 to 34 mice were rapidly dissected postcervical dislocation and washed with ice-cold 10 mM Hepes-HCl in Hank's balanced salt solution (HBSS). The tissue then was dounce homogenized (40 strokes, Corning 7724T3) in 1 mL of lysis buffer consisting of 25 mM Hepes-HCl pH 7.3, 150 mM KCl, 5 mM $MgCl_2$, 0.5 mM dithiothreitol (DTT), 100 $\mu g \cdot mL^{-1}$ cycloheximide, 10 $U \cdot mL^{-1}$ SUPERase-In, and 1X Halt protease and phosphatase inhibitor. The lysate was centrifuged at 2,000 × *g* (4 °C) for 10 min and Nonidet P-40 (Sigma I8896) was added to a final concentration of 1% to the supernatant, which then was centrifuged at 10,000 × *g* (4 °C) for 5 min. The final supernatant was gently layered onto 10 to 50% sucrose density gradients prepared in 25 mM Hepes-HCl pH 7.3, 150 mM KCl, 5 mM $MgCl_2$, 0.5 mM DTT, and 10 $U \cdot mL^{-1}$ SUPERase-In. The gradients were ultracentrifuged at 35,000 rpm on a SW41-Ti rotor for 2.5 h (4 °C). To obtain polysome profiles, gradients then were fractionated with continuous monitoring of ultraviolet (UV) absorbance at 254 nm in a Biocomp Piston Gradient Fractionator.

Isolation of RF and Total RNA. Cortices from P29 to 34 WT ($n = 4$), FXS ($n = 5$), S6K1 ($n = 3$), and DKO ($n = 3$) animals were rapidly dissected, washed with ice-cold 10 mM Hepes-HCl pH 7.3 in HBSS, then lysed by dounce homogenization (40 strokes) in 25 mM Hepes-HCl pH 7.3, 150 mM KCl, 5 mM $MgCl_2$, 0.5 mM DTT, 100 $\mu g \cdot mL^{-1}$ cycloheximide, and protease/phosphatase inhibitors on ice. Lysates were centrifuged at 2,000 × *g* for 10 min (4 °C) to remove cellular debris and nuclei. A total of 10 A260 units of the supernatant were incubated with 1 μg RNase A and 600 units RNase T1, with gentle rotation for 30 min at room temperature. RNase digestion was stopped by placing the tubes on ice subsequent to the addition 600 U SUPERase-In to each reaction. The RNase digested lysates then were supplemented with Nonidet P-40 to a final concentration of 1%. After incubating on ice for 5 min, the lysates were centrifuged at 10,000 × *g* for 5 min, and the supernatants layered on a 10 to 50% sucrose density gradient prepared in 25 mM Hepes-HCl pH 7.3, 150 mM KCl, 5 mM $MgCl_2$, 0.5 mM DTT, and 10 $U \cdot mL^{-1}$ SUPERase-In. The gradients were ultracentrifuged for 2.5 h (4 °C) in a SW41Ti rotor (Beckman Coulter) at 35,000 rpm, after which they were fractionated on a Biocomp Piston Gradient Fractionator with continuous UV absorbance monitoring (254 nm) on the EM1 UV Monitor (Bio-Rad). Monosome fractions

were isolated, and RNA extracted with TRIzol-LS. For total RNA isolation (n = 4 each of WT, FXS, S6K1, and DKO), cortices were lysed as described. Lysates were supplemented with 600 U SUPERase-In and 1% Nonidet P-40, the RNase digestion step skipped, and 10,000 × g supernatant isolated. The cortex from a single mouse was used to prepare one RF or RNA-Seq high-throughput sequencing library.

High-Throughput Sequencing Library Preparation. RFs were converted to sequencing libraries as described previously (41). Briefly, ribosomal RNA was depleted from monosome fractions with Ribo-Zero Gold, after which 26 to 34 nt long monosomal RNA was fractionated out using a 15% Urea-Page gel. The excised RNA was 3′ dephosphorylated, ligated to a preadenylated adapter, reverse transcribed, circularized, and PCR amplified to generate strand-specific sequencing libraries. For RNA-Seq, the TruSeq-stranded mRNA kit (Illumina) was employed to select polyA-tailed RNAs and convert them to strand-specific sequencing libraries.

High-Throughput Sequencing Data Processing. Ribosome profiling reads were demultiplexed using in-house scripts. Sequencing adapters were removed using CutAdapt. Reads aligning to ribosomal and tRNA were excised using Bowtie2. The remaining reads were aligned to the mouse genome (mm10) using TopHat2, with segment length set at 12. PCR duplicates were removed from alignments using unique molecular identifier (UMI) information present in the reads. All reads with nonunique alignments were also discarded. RF abundance was calculated by directly aligning the remaining reads specifically to the CDS region of *Mus musculus* protein-coding genes using RSEM. To calculate mRNA expression deriving from CDS-derived reads, RNA-Seq reads were processed identically, except removal of duplicate reads was not carried out because of the lack of UMI information in RNA-Seq libraries.

To construct the RF profile of an individual mRNA, all 5′ alignments at each position along the mRNA was obtained with Plastid (42). The total number of alignments at each position derived from a given library was normalized by the size factor computed by DESeq2 for that library. Rolling means of the average normalized counts of all samples of the same genotype were plotted to reveal the average RF profile of the mRNA.

Statistical Analysis of RF Expression and mRNA Expression. DESeq2 (43) was used to model the RF and RNA-Seq data. Gene level expression/abundance estimated by RSEM for RF and RNA-Seq were collated into respective count matrices and used as input for DESeq2. Following the authors' recommendations, we modeled data from all four genotypes together. Genes with less than 1 count per million in any of libraries were excluded from the analysis. The threshold for differential expression was set at an FDR of 0.1.

Gene Set Enrichment Analysis. We used the R package fgsea to carry out gene set enrichment analysis (44). Genes were preranked by the Wald test statistic computed when testing for differential expression in DESeq2. Only significantly different genes in the RF or RNA-Seq assays at FDR < 0.1 were used in this analysis.

Gene Set Overlap Analysis. We used the hypergeometric test to calculate the probability that the genes differentially expressed in FXS cortices in either RF or mRNA expressions overlapped by chance with the genes thought to be binding targets of FMRP. Specifically, we used the phyper function in R, with the total number of genes set by the number of genes that were included in the DESeq2 analysis (12,083 for RF and 12,876 for RNA-Seq).

Division of mRNAs into CDS Length Bins. Annotations for all *M. musculus* protein-coding genes in RefSeq were obtained from University of California, Santa Cruz table browser. Using these annotations, the CDS region of the mRNAs was extracted using in-house scripts. This truncated transcriptome was used to prepare references for RSEM. When calculating expression, RSEM summates the length of all mRNA isoforms of the gene into an "effective length" for that gene. The effective lengths were log transformed, and its histogram was divided at regular intervals to categorize genes into six CDS length bins. To divide mRNAs into 50 bins evenly, the total number of robustly expressed mRNAs (counts per million > 1 for all samples) were divided by 50, and the number of genes indicated by the remainder was removed at random. For example, 33 genes were removed at random from 12,033 genes to ensure that each length bin contained 240 mRNAs.

Primary Neuron Culture. Primary neuron cultures were obtained from E16.5 WT and FXS mice. Cultures were prepared as previously described (45). Briefly, dams were euthanized by CO_2 inhalation in accordance with the Institutional Animal Care and Use Committee guidelines. Embryos were rapidly isolated into ice-cold HBSS supplemented with glucose and their cortices and hippocampi dissected out. The embryonic tissue was trypsinized, triturated, and plated onto either cell culture dishes or coverslips coated with poly-D-lysine and laminin. Neurons were cultured in Neurobasal media supplemented with B27, Glutamax, and penicillin/streptomycin in a 5% CO_2 incubator at 37 °C. Fresh media was supplemented every 3 d. All experiments were carried out on days in vitro (DIV) seven to eight neurons. To keep the environment constant, WT and FXS cultures were plated on different wells of the same multiwell plate, and all experiments were carried out simultaneously for WT and FXS neurons.

Lentiviral Transduction. Lentivirus constitutively expressing full-length N-terminal, Flag-tagged human *FMR1* and a control lentivirus constitutively expressing EGFP were produced at Emory Viral Vector Core. Both constructs are cloned into the pFUGW plasmid (45). Infection was carried out by incubating DIV 2 neurons with lentivirus diluted in conditioned media for 24 h, after which the viral media was replaced with previously saved conditioned media.

Measurement of De Novo Protein Synthesis (SUnSET). DIV seven to eight WT and FXS primary neurons were treated with 0.5 $\mu g \cdot mL^{-1}$ puromycin in conditioned media for 15 min. Cells then were washed once with ice-cold phosphate-buffered saline (PBS) and lysed in radioimmunoprecipitation assay (RIPA) buffer supplemented with 1X Halt protease and phosphatase inhibitor. Lysates were flash frozen, processed as described, and analyzed on Western blots.

ES. DIV seven to eight WT and FXS primary neurons were treated with 5 $\mu g \cdot mL^{-1}$ HHT to induce runoff elongation. After 0, 8, or 16 min of treatment, the runoff media was replaced with a mix of 5 $\mu g \cdot mL^{-1}$ HHT and 50 $\mu g \cdot mL^{-1}$ puromycin for 15 min to continue inhibiting translation initiation while simultaneously measuring the functional output of only the elongation phase of protein synthesis. Cells then were washed with ice-cold PBS and lysed in RIPA buffer supplemented with 1X Halt. All treatments were carried out in 50% conditioned media. Lysates were flash frozen, processed as described, and analyzed on Western blots.

Runoff-RPM. DIV seven to eight WT and FXS primary neurons were treated either with vehicle (0.1% DMSO) or 10 $\mu g \cdot mL^{-1}$ PF-4708671, diluted from a freshly prepared 10 $mg \cdot mL^{-1}$ stock in DMSO. After 1 h of drug treatment, runoff elongation was carried out for 0, 8, or 16 min by replacing the drug treatment media with runoff media, which consisted of 5 $\mu g \cdot mL^{-1}$ HHT and vehicle/10 $\mu g \cdot mL^{-1}$ PF-4708671. At the end of each time point, runoff media was aspirated out and replaced with labeling media made of 5 $\mu g \cdot mL^{-1}$ HHT, 200 μM emetine, 50 $\mu g \cdot mL^{-1}$ puromycin, and vehicle/10 $\mu g \cdot mL^{-1}$ PF-4708671. Labeling was carried out for 5 min, after which neurons were washed with ice-cold PBS and lysed with RIPA buffer supplemented with 1X Halt. Lysates were flash frozen, processed as described, and analyzed on Western blots. The initial S6K1 inhibitor treatment was carried out in 100% conditioned media, and all other treatments were carried out in 50% conditioned media.

For imaging, experiments were carried out identically, except after labeling, coverslips with neurons were washed with room temperature 0.004% saponin + 5 $\mu g \cdot mL^{-1}$ HHT + 200 μM emetine in HBSS for 1 min to prepermeabilize the cells. The coverslips then were washed rapidly with warm (~37 °C) HBSS + 5 $\mu g \cdot mL^{-1}$ HHT + 200 μM emetine twice to remove unbound puromycin, after which they were fixed with 4% PFA in PBS for 20 min at room temperature.

Runoff-RPM in HEK Cells. Runoff-RPM was carried in HEK cells as it was in neurons, except 0.015% digitonin was used to prepermeabilize cells before fixation. For anisomycin controls, RPM labeling was carried out in 200 μM emetine, 50 $\mu g \cdot mL^{-1}$ puromycin, and 50 $\mu g \cdot mL^{-1}$ anisomycin after pretreatment with 10 $\mu g \cdot mL^{-1}$ anisomycin for 15 min.

Western Blotting. Flash-frozen lysates were thawed and briefly sonicated on ice and centrifuged at 20,000 × g for 10 min (4 °C). The supernatant was saved, and its protein concentration was measured using the BCA assay. 6× Laemmli buffer (Boston Bioproducts #BP-111R) was added to the sample and mixed thoroughly, after which the sample was boiled for 6 min. A total of 15

to 20 μg of protein from each sample was loaded on 4 to 12% Bolt Bis-Tris gradient gels (Invitrogen), followed by dry transfer onto nitrocellulose membranes. Membranes were blocked for 90 min with 5% milk in Tris-buffered saline supplemented with 0.1% Tween-20 (TBST). Membranes were then probed overnight (4 °C) with 1:1,000 anti-puromycin antibody (MABE343, Millipore) in 5% milk TBST with gentle rotation. After four vigorous 5-min washes in TBST, the membranes were incubated with 1:10,000 HRP conjugated anti-mouse IgG antibody for 1 h in 5% milk TBST at room temperature. Membranes were then washed again four times vigorously in TBST and imaged on the FluorChem-E platform (Protein Simple). Enhanced chemiluminescence and exposures were set to obtain signals in the linear range. Membranes were then stripped, reblocked with 5% milk TBST, and cut into three pieces with horizontal incisions at ∼60 and 37 kDA. The top portion of the membrane was probed with 1:1,000 anti-FMRP antibody (Biolegend 834601), the middle portion with 1:1,000 anti–γ-Tubulin (Sigma T5326), and the bottom with 1:1,000 anti-phospho S6 Ser-240/244 antibody (Cell Signaling 5364), all in 5% milk TBST. Membranes were imaged for the respective antibodies again as described.

For examination of protein abundances of specific proteins in FXS and WT mice, cortical lysates were obtained as described in *Isolation of RF and Total RNA*. The following antibodies were used: Herc1 (Invitrogen A301-904A-T), Dst (Invitrogen PA5-106906), Plec1 (Cell Signaling 12254S), Adcy1 (Novus NBP2-92583), and Eif1 (Invitrogen MA1-077). To examine Zmiz1 expression (Millipore MABN250), whole-cell lysates were obtained by sonicating flash-frozen cortical tissue in RIPA buffer supplemented with 1X Halt. All antibodies were used at 1:1,000 dilution.

Microscopy. Coverslip-grown neurons fixed after runoff-RPM were washed with PBS twice, permeabilized with 0.2% Triton-X in PBS for 5 min, and blocked with 5% BSA in PBS for 30 min. Coverslips were incubated with 1:1,000 anti-puromycin conjugated to Alexa Fluor 488 (Millipore MABE343-AF488), and 1:500 Ch. anti-Map2 (Encor Biotech CPCA-MAP2) overnight (4 °C) in 1% BSA in PBS. Subsequent to three 5 min PBS washes, coverslips were probed with 1:200 anti-chicken IgG conjugated with Alexa Fluor 647 in 1% BSA for 1 h at room temperature. After another three washes in PBS, coverslips were mounted and imaged on a Leica SP8 confocal microscope. All microscopy parameters including laser intensities, gains, and offsets were optimized on WT baseline (0 min of runoff), after which every coverslip of either genotype was imaged using the exact same settings.

Analysis of Rate of Loss in Runoff-RPM Data. For Western blots, because we were able to load samples from all experimental conditions and their multiple runoff durations on a single gel, the RPM signal of a given condition in a given membrane was compared against its own baseline in the same membrane to produce the final dataset.

For immunofluorescence images, it was not possible to examine all conditions and their associated runoff durations on the same coverslip. Therefore, we first quantified the puromycin immunofluorescence in individual cells across all experimental conditions and runoff durations over two replicates. We then sampled 10 cells (without replacement) from each condition and computed their averages. We used this set of averages as a complete experimental group (i.e., we computed the group-wise reduction in RPM signal against the baseline average RPM signal within this randomly sampled set of measurements). We repeated this process 50 times to produce the final dataset.

Data Availability. All data used in the analysis have been deposited under record number GSE143659 in the National Center for Biotechnology Information Gene Expression Omnibus database. All other study data are included in the article and/or *SI Appendix*.

ACKNOWLEDGMENTS. We thank Thomas Dever (NIH) for a critical reading of our manuscript; Leila Myrick and Stephen T. Warren (Emory University) for generously providing the human full-length FMRP expression plasmids; and Botao Liu, Huan Shu, Elisa Donnard, and Joel Richter (University of Massachusetts Medical School) for a demonstration of and technical advice on ribosome profiling library preparation and data analysis. This work was primarily supported by NIH grants to E.K. (NS034007, NS047384, and HD082013). We also acknowledge NIH funding to the Genome Technology Center at New York University Langone Health (P30CA016087).

1. M. Qin, J. Kang, T. V. Burlin, C. Jiang, C. B. Smith, Postadolescent changes in regional cerebral protein synthesis: An in vivo study in the FMR1 null mouse. *J. Neurosci.* **25**, 5087–5095 (2005).
2. M. S. Sidorov, B. D. Auerbach, M. F. Bear, Fragile X mental retardation protein and synaptic plasticity. *Mol. Brain* **6**, 15 (2013).
3. J. C. Darnell, E. Klann, The translation of translational control by FMRP: Therapeutic targets for FXS. *Nat. Neurosci.* **16**, 1530–1536 (2013).
4. A. Bhattacharya *et al*., Genetic removal of p70 S6 kinase 1 corrects molecular, synaptic, and behavioral phenotypes in fragile X syndrome mice. *Neuron* **76**, 325–337 (2012).
5. S. R. Thomson *et al*., Cell-type-specific translation profiling reveals a novel strategy for treating fragile X syndrome. *Neuron* **95**, 550–563.e5 (2017).
6. L. Ceolin *et al*., Cell type-specific mRNA dysregulation in hippocampal CA1 pyramidal neurons of the fragile X syndrome mouse model. *Front. Mol. Neurosci.* **10**, 340 (2017).
7. S. Das Sharma *et al*., Widespread alterations in translation elongation in the brain of juvenile Fmr1 knockout mice. *Cell Rep.* **26**, 3313–3322.e5 (2019).
8. E. J. Greenblatt, A. C. Spradling, Fragile X mental retardation 1 gene enhances the translation of large autism-related proteins. *Science* **361**, 709–712 (2018).
9. N. T. Ingolia, S. Ghaemmaghami, J. R. S. Newman, J. S. Weissman, Genome-wide analysis in vivo of translation with nucleotide resolution using ribosome profiling. *Science* **324**, 218–223 (2009).
10. J. C. Darnell *et al*., FMRP stalls ribosomal translocation on mRNAs linked to synaptic function and autism. *Cell* **146**, 247–261 (2011).
11. E. Chen, M. R. Sharma, X. Shi, R. K. Agrawal, S. Joseph, Fragile X mental retardation protein regulates translation by binding directly to the ribosome. *Mol. Cell* **54**, 407–417 (2014).
12. E. K. Schmidt, G. Clavarino, M. Ceppi, P. Pierre, SUnSET, a nonradioactive method to monitor protein synthesis. *Nat. Methods* **6**, 275–277 (2009).
13. M. V. Gerashchenko, Z. Peterfi, S. H. Yim, V. N. Gladyshev, Translation elongation rate varies among organs and decreases with age. *Nucleic Acids Res.* **49**, e9 (2021).
14. T. Udagawa *et al*., Genetic and acute CPEB1 depletion ameliorate fragile X pathophysiology. *Nat. Med.* **19**, 1473–1477 (2013).
15. A. David, J. R. Bennink, J. W. Yewdell, Emetine optimally facilitates nascent chain puromycylation and potentiates the ribopuromycylation method (RPM) applied to inert cells. *Histochem. Cell Biol.* **139**, 501–504 (2013).
16. Y. Arava *et al*., Genome-wide analysis of mRNA translation profiles in *Saccharomyces cerevisiae*. *Proc. Natl. Acad. Sci. U.S.A.* **100**, 3889–3894 (2003).
17. L. D. Fernandes, A. P. S. de Moura, L. Ciandrini, Gene length as a regulator for ribosome recruitment and protein synthesis: Theoretical insights. *Sci. Rep.* **7**, 17409 (2017).
18. E. Eisenberg, E. Y. Levanon, Human housekeeping genes are compact. *Trends Genet.* **19**, 362–365 (2003).
19. C. I. Castillo-Davis, S. L. Mekhedov, D. L. Hartl, E. V. Koonin, F. A. Kondrashov, Selection for short introns in highly expressed genes. *Nat. Genet.* **31**, 415–418 (2002).
20. J. Guo, X. Lian, J. Zhong, T. Wang, G. Zhang, Length-dependent translation initiation benefits the functional proteome of human cells. *Mol. Biosyst.* **11**, 370–378 (2015).
21. J. W. B. Hershey, N. Sonenberg, M. B. Mathews, Principles of translational control. *Cold Spring Harb. Perspect. Biol.* **11**, a032607 (2019).
22. R. L. Ouwenga, J. Dougherty, Fmrp targets or not: Long, highly brain-expressed genes tend to be implicated in autism and brain disorders. *Mol. Autism* **6**, 16 (2015).
23. S. Gholizadeh, S. K. Halder, D. R. Hampson, Expression of fragile X mental retardation protein in neurons and glia of the developing and adult mouse brain. *Brain Res.* **1596**, 22–30 (2015).
24. C. S. von Bartheld, J. Bahney, S. Herculano-Houzel, The search for true numbers of neurons and glial cells in the human brain: A review of 150 years of cell counting. *J. Comp. Neurol.* **524**, 3865–3895 (2016).
25. A. Sharma *et al*., Dysregulation of mTOR signaling in fragile X syndrome. *J. Neurosci.* **30**, 694–702 (2010).
26. K. M. Hannan *et al*., mTOR-dependent regulation of ribosomal gene transcription requires S6K1 and is mediated by phosphorylation of the carboxy-terminal activation domain of the nucleolar transcription factor UBF. *Mol. Cell. Biol.* **23**, 8862–8877 (2003).
27. C. Chauvin *et al*., Ribosomal protein S6 kinase activity controls the ribosome biogenesis transcriptional program. *Oncogene* **33**, 474–483 (2014).
28. R. P. de Groot, L. M. Ballou, P. Sassone-Corsi, Positive regulation of the cAMP-responsive activator CREM by the p70 S6 kinase: An alternative route to mitogen-induced gene expression. *Cell* **79**, 81–91 (1994).
29. C. J. Richardson *et al*., SKAR is a specific target of S6 kinase 1 in cell growth control. *Curr. Biol.* **14**, 1540–1549 (2004).
30. I. Napoli *et al*., The fragile X syndrome protein represses activity-dependent translation through CYFIP1, a new 4E-BP. *Cell* **134**, 1042–1054 (2008).
31. C. C. Thoreen *et al*., A unifying model for mTORC1-mediated regulation of mRNA translation. *Nature* **485**, 109–113 (2012).

32. M. J. Zylka, J. M. Simon, B. D. Philpot, Gene length matters in neurons. *Neuron* **86**, 353–355 (2015).
33. G. Hanson, N. Alhusaini, N. Morris, T. Sweet, J. Coller, Translation elongation and mRNA stability are coupled through the ribosomal A-site. *RNA* **24**, 1377–1389 (2018).
34. A. Narula, J. Ellis, J. M. Taliaferro, O. S. Rissland, Coding regions affect mRNA stability in human cells. *RNA* **25**, 1751–1764 (2019).
35. L. Lisi, P. Navarra, D. L. Feinstein, C. Dello Russo, The mTOR kinase inhibitor rapamycin decreases iNOS mRNA stability in astrocytes. *J. Neuroinflammation* **8**, 1 (2011).
36. N. M. Sosanya *et al*., Degradation of high affinity HuD targets releases Kv1.1 mRNA from miR-129 repression by mTORC1. *J. Cell Biol.* **202**, 53–69 (2013).
37. Y. Park, A. Reyna-Neyra, L. Philippe, C. C. Thoreen, mTORC1 balances cellular amino acid supply with demand for protein synthesis through post-transcriptional control of ATF4. *Cell Rep.* **19**, 1083–1090 (2017).
38. M. Laplante, D. M. Sabatini, Regulation of mTORC1 and its impact on gene expression at a glance. *J. Cell Sci.* **126**, 1713–1719 (2013).
39. W. Li *et al*., Structural basis for selective stalling of human ribosome nascent chain complexes by a drug-like molecule. *Nat. Struct. Mol. Biol.* **26**, 501–509 (2019).
40. National Research Council, *Guide for the Care and Use of Laboratory Animals* (National Academies Press, Washington, DC, 8th Ed., 2011).
41. C. Cenik *et al*., Integrative analysis of RNA, translation and protein levels reveals distinct regulatory variation across humans. *Genome Res.* **25**, 1610–1621 (2015).
42. J. G. Dunn, J. S. Weissman, Plastid: Nucleotide-resolution analysis of next-generation sequencing and genomics data. *BMC Genomics* **17**, 958 (2016).
43. M. I. Love, W. Huber, S. Anders, Moderated estimation of fold change and dispersion for RNA-seq data with DESeq2. *Genome Biol.* **15**, 550 (2014).
44. A. A. Sergushichev, An algorithm for fast preranked gene set enrichment analysis using cumulative statistic calculation. *bioRxiv* [Preprint] (2016). https://www.biorxiv.org/content/10.1101/060012v1 (Accessed 15 October 2019).
45. L. K. Myrick *et al*., Fragile X syndrome due to a missense mutation. *Eur. J. Hum. Genet.* **22**, 1185–1189 (2014).